Enhanced Catalytic Activity of a de novo Enzyme in a Coacervate Phase

Eugénie Kluczka, Valentin Rinaldo, Angélique Coutable-Pennarun, Claire Stines-Chaumeil, J L Ross Anderson, Nicolas Martin

Enhanced Catalytic Activity of a de novo Enzyme in a Coacervate Phase

Eugénie Kluczka,[a] Valentin Rinaldo,[a] Angélique Coutable-Pennarun,[b] Claire Stines-Chaumeil,[a] J. L. Ross Anderson,[b],* Nicolas Martin[a],*

[a] E. Kluczka, V. Rinaldo, Dr. C. Stines-Chaumeil, Dr. N. Martin*
Univ. Bordeaux, CNRS, Centre de Recherche Paul Pascal, UMR 5031
115 Avenue du Dr. Albert Schweitzer, 33600 Pessac (France)
E-mail: nicolas.martin@crpp.cnrs.fr

[b] Dr. A. Coutable-Pennarun, Prof. J. L. R. Anderson*
School of Biochemistry, University of Bristol
Bristol BS8 1TD (UK)
and Bristol BioDesign Institute, University of Bristol
Life Sciences Building, Bristol BS8 1TQ (UK)
E-mail: ross.anderson@bristol.ac.uk

"This is the accepted version of the following article: E. Kluczka *et al.*, *ChemCatChem*, **2024**, e202400558**, which has been published in final form at** https://chemistry-europe.onlinelibrary.wiley.com/doi/full/10.1002/cctc.202400558

Abstract: Biomolecular condensates are membraneless organelles that orchestrate various metabolic pathways in living cells. Understanding how these crowded structures regulate enzyme reactions remains yet challenging due to their dynamic and intricate nature. Coacervate microdroplets formed by associative liquid-liquid phase separation of oppositely charged polyions have emerged as relevant condensate models to study enzyme catalysis. Enzyme reactions within these droplets show altered kinetics, influenced by factors such as enzyme and substrate partitioning, crowding, and interactions with coacervate components; it is often challenging to disentangle the contributions of each. Here, we investigate the peroxidase activity of a de novo enzyme within polysaccharide-based coacervates. By comparing the reaction kinetics in buffer, in a suspension of coacervates and in the bulk coacervate phase collected after centrifugation of the droplets, we show that the coacervate phase significantly increases the enzyme catalytic efficiency. We demonstrate that the main origin of this enhanced activity lies in macromolecular crowding coupled to changes in the conformational dynamics of the enzyme within the coacervate environment. Altogether, these findings underline the crucial role of the coacervate matrix in enzyme catalysis, beyond simple partitioning effects. The observed boost in enzyme activity within the coacervate phase provides insights for designing biocatalytically active synthetic organelles.

Introduction

Biomolecular condensates are an emerging class of organelles that are increasingly recognized as key organizers of intracellular contents.[1] These membraneless droplets form by liquid-liquid phase separation involving weak multivalent interactions between proteins (often containing intrinsically disordered regions) or between proteins and RNA. Their ability to selectively sequester biomolecules allows them to promote or inhibit catalytic reactions by localizing enzymes in the cytoplasm, and therefore to direct metabolic fluxes and signalling cascades.[2, 3] Several hypotheses have been put forward to explain the effect of biomolecular condensates on enzyme catalysis, such as enzyme and substrate co-localization or macromolecular crowding.[2] However, the intrinsic biochemical complexity and out-of-equilibrium state of natural condensates often make it challenging to dissect the mechanisms by which these organelles regulate enzyme reactions in vivo. The design of synthetic organelles capable of fine tuning enzyme activity would open yet new avenues to regulate biocatalysis both in vivo and in vitro.[4-6]

Complex coacervate microdroplets produced by associative liquid-liquid phase separation between oppositely charged polyions represent relevant in vitro models of membraneless organelles.[7-9] Despite the greater simplicity of their chemical composition and interactions at play, coacervate droplets recapitulate essential features of

biomolecular condensates, including their physicochemical properties (liquid-like nature, viscoelasticity…) and their capacity to selectively sequester biomolecules.[7] [10, 11] Coacervates thus appear as an appealing platform to elucidate fundamental principles of enzyme catalysis in condensate-like environments. Several enzymatic reactions have already been implemented in coacervate droplets using well-known natural enzymes, showing either enhanced or reduced reaction kinetics. Acceleration of enzyme reactions has often been attributed to enzyme and substrate accumulation and co-localization within coacervate droplets.[12-14] Beyond the law of the mass action, other factors such as macromolecular crowding, chemical partitioning, or interactions between enzymes and the coacervates' components also play an important role on enzyme catalysis. For instance, crowding can lead to slower enzyme kinetics due to reduced diffusion[15] or accelerate reactions based on excluded volume effects[16] (including shifting the equilibrium of protein-substrate interactions or enzyme conformational dynamics and hydration shell around enzymes); product build-up within the droplets can result in product inhibition;[17] interactions with the coacervates' components can trap enzymes in an inactive conformation,[18] reduce its thermodynamic stability,[11a] alter the enzyme mobility,[19] or affect the affinity of enzymes for their substrates.[15] [20]

A comprehensive understanding of the basic principles governing how coacervates impact enzyme reactions still encounters challenges due to the intricate interplay of multiple context-dependent factors. In particular, most of the reported enzyme reactions have been performed in suspensions of coacervate microdroplets, namely, under conditions where molecular exchange between the droplets and the surrounding aqueous phase occurs. While the coexistence of these two phases can prove important for substrate supply and product removal,[21] it also makes it challenging to decouple the specific roles of the coacervate matrix and of partitioning on enzyme activities. Notably, the exact amount of species in the coacervate droplets is often not accurately determined, and activities in the bulk coacervate phase, collected after centrifugation of the droplets suspension, are rarely quantified. The direct impact of the coacervate environment on enzyme activities thus remains poorly understood. Last, reports on biocatalysis within coacervates have exclusively focused on canonical enzymes, while the untapped potential of non-natural enzymes, with structures and functions amenable to engineering, remains unexplored in this context.

Here, we investigate the effect of a polysaccharide-based complex coacervate phase on the activity of C45, a rationally designed four-helical bundle protein that contains a covalently linked heme and functions as a catalytically proficient and promiscuous peroxidase.[22-25] We first show that the coacervate environment provides a fluid, albeit crowded, environment for C45, then quantitatively compare the reaction kinetics at varying substrate concentrations in the coacervate droplet suspension and in the bulk coacervate phase. Fitting of the data reveals that the coacervate environment increases the Michaelis-Menten constant due to electrostatic interactions between C45 and polysaccharide chains. More excitingly, our data reveal that the bulk coacervate phase, but not the coacervate droplet suspension, induces a significant increase in the catalytic efficiency of C45 compared to standard buffer conditions. We show that this increase stems from a combination of macromolecular crowding and a decrease of the enzyme's conformational dynamics in the coacervate phase. Overall, our results point to the key role of the coacervate matrix on enzyme catalysis beyond the commonly ascribed up-concentration effect. Our data thus emphasize the importance of quantifying enzyme activities in both coacervate droplet suspensions and coacervate bulk phases to elucidate the various contributions of enzyme confinement within coacervates on reactions kinetics. The reported up-regulation of peroxidase activity of a de novo enzyme in coacervates also provides design principles to develop biocatalytically efficient synthetic organelles.

Results and Discussion

Coacervate droplets accumulate and provide a fluid environment to a de novo peroxidase enzyme

Our coacervate system was produced by mixing two oppositely charged polysaccharides, diethylenediamine (DEAE)-dextran (M_w = 500 kg.mol^{-1}) and carboxymethyl (CM)-dextran (M_w = 10-20 kg.mol^{-1}), in 20 mM sodium phosphate buffer at pH 7.4 (**Figure 1a**). Turbidity screening at varying relative polymer concentrations revealed that the maximum turbidity (corresponding to optimal coacervation conditions) occurred for a DEAE-:CM-dextran weight ratio of 1:3 (**Figure 1b** and **Supplementary Figure 1a**). We therefore used this ratio throughout our study. Optical microscopy images of the turbid suspension produced at 3 mg.mL^{-1} DEAE-dextran and 9 mg.mL^{-1} CM-dextran

confirmed the presence of polydisperse microdroplets (**Figure 1c**) that fused together on contact, as expected for a liquid phase, with an inverse capillary viscosity, η/γ, of 19.8 ± 1.5 ms.μm^{-1} (**Supplementary Figure 2**). This value was ca. 50-fold lower to that reported for typical biomolecular condensates found in living cells.[26] The droplets were highly hydrated (composed of 86.0 ± 0.2 wt% of water) and contained a total polymer concentration of 144 ± 2 mg.mL^{-1}, as estimated by measurements of the dry weight of a given volume of bulk coacervate phase (see Methods). Addition of sodium chloride salt above 50 mM resulted in droplet disassembly (**Supplementary Figure 1b**), which confirmed that coacervation was driven by attractive electrostatic interactions between the two polyelectrolytes. Centrifugation of the droplets suspension resulted in a macroscopic phase separation into a lower bulk (polymer-rich) coacervate phase and an upper (dilute) supernatant phase that could be collected separately (**Figure 1b**).

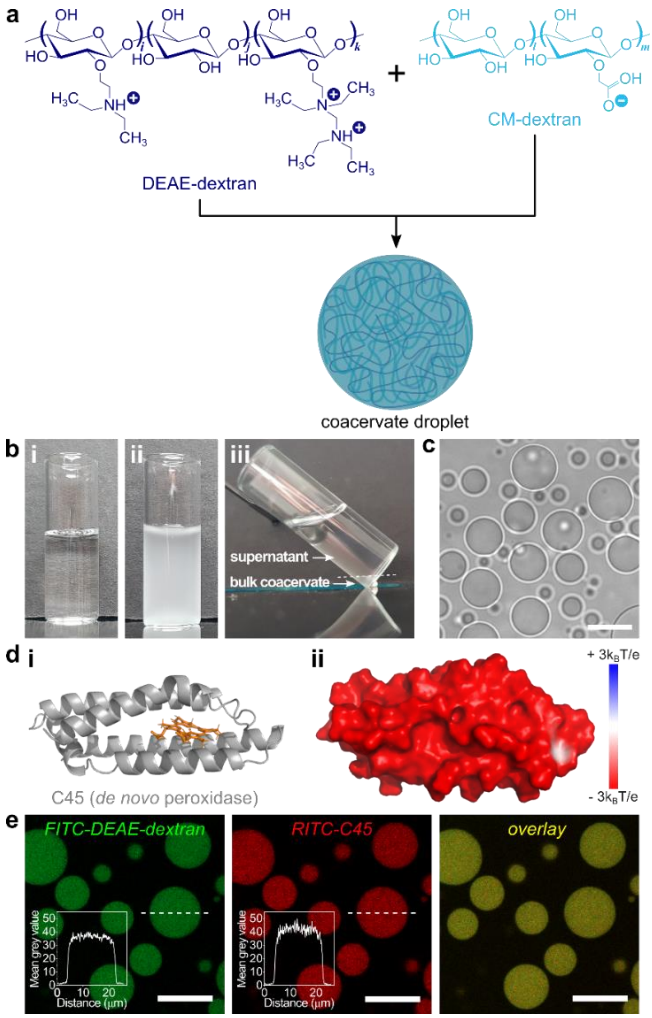

Figure 1. a, Chemical structure of the two oppositely charged polysaccharides used to assemble coacervate microdroplets, DEAE- and CM-dextran, and scheme showing the formation of coacervates upon their mixing. **b**, Pictures of the samples before (i) and after (ii) polymer mixing in 20 mM sodium phosphate buffer pH 7.4 (using 3 mg.mL^{-1} DEAE-dextran and 9 mg.mL^{-1} CM-dextran), showing a clear solution and turbid suspension of coacervate droplets, respectively. The latter undergoes macroscopic phase separation over time or via centrifugation to produce a bulk coacervate phase (lower phase) separated from a dilute supernatant (upper phase) (iii). These two phases can be collected separately by pipetting. **c**, Bright-field optical microscopy image of the DEAE-/CM-dextran coacervate microdroplets produced as in **b**. Scale bar, 20 μm. **d**, 3D structure (i) and electrostatic surface charge potential at pH 7.5 (ii) of the de novo C45 enzyme. The ferrous heme covalently linked to the protein is shown in orange in (i). **e**, Confocal fluorescence microscopy images of DEAE-/CM-dextran coacervate droplets produced as in **c** and doped with FITC-labelled DEAE-dextran (70 kDa, 0.1 mg.mL^{-1}) and RITC-labelled C45 (1 μM), and line profiles of red and green fluorescence, respectively, along the dotted white lines. Scale bars, 20 μm.

We then added the C45 enzyme to the coacervate droplet suspension, and determined its spontaneous uptake in the droplets by UV/vis spectroscopy after centrifugation using the Soret band at 406 nm. The measured partition coefficient, namely, the ratio of C45 concentration in the coacervate vs. supernatant phases, was 150 ± 81, indicating that the enzyme strongly accumulated in the coacervate droplets. This high partitioning was likely attributed to attractive electrostatic interactions between positively charged DEAE-dextran chains and negatively charged C45 (**Figure 1d**, isoelectric point, pI, of ca. 4.1). This hypothesis was corroborated by the fact that DEAE-dextran and C45 could undergo complex coacervation at higher concentrations without the addition of CM-dextran due to attractive electrostatic interactions between the two species (**Supplementary Figure 3**), a behaviour widely reported for natural globular proteins and polyelectrolytes.[27]

Confocal fluorescence microscopy performed on DEAE-/CM-dextran coacervate droplets doped with fluorescein-isothiocyanate (FITC)-labelled DEAE-dextran (M_w = 70 kg.mol^{-1}, 0.1 mg.mL^{-1}) after addition of rhodamine isothiocyanate (RITC)-labelled C45 (1 µM) confirmed that the labelled enzymes spontaneously co-localized with the polysaccharide chains and accumulated in the droplets (**Figure 1e**). Fluorescence recovery after photobleaching (FRAP) on coacervates containing RITC-C45 further revealed that the enzyme remained mobile in the coacervate phase with an apparent diffusion coefficient of 2.2 ± 0.5 µm^2.s^{-1} (**Supplementary Figure 4**). This value was ca. 50-fold lower than in pure buffer (using the Stokes-Einstein relationship and a hydrodynamic radius for C45 of 2 nm), indicating that, albeit highly fluid, the coacervate matrix restricted the diffusion of enzymes, as expected in this crowded polymer-rich environment.

Overall, these results show that the de novo enzyme C45 is strongly partitioned inside DEAE-/CM-dextran coacervate microdroplets, remains mobile in the coacervate matrix but exhibits a reduced diffusion coefficient compared to pure buffer, which is likely attributed to a combination of macromolecular crowding and electrostatic binding to DEAE-dextran chains in the coacervate micro-environment.

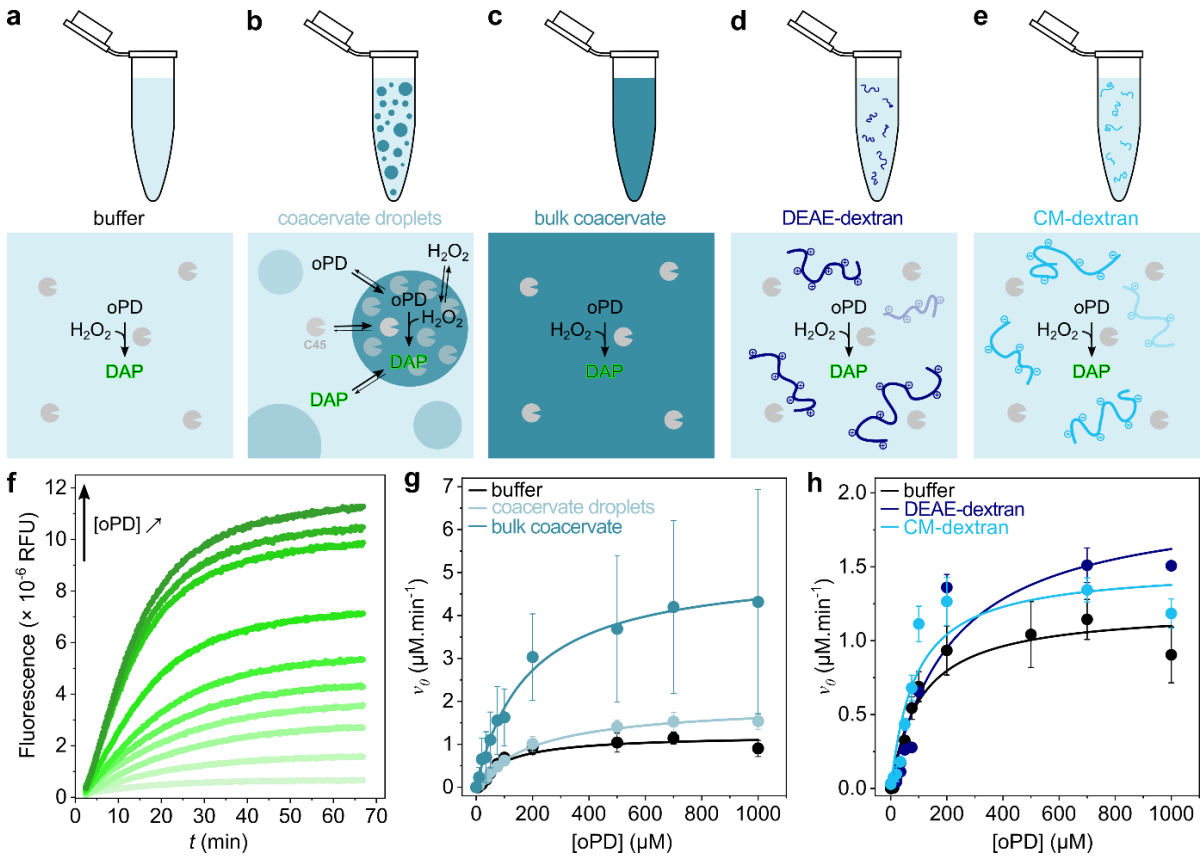

Figure 2. a-e, Schematic representation of the reaction conditions in a test tube (top) and of the distribution of reactants in the different milieus (bottom). Buffer, DEAE-dextran, CM-dextran: enzyme and substrates are mixed together in 20 mM sodium phosphate buffer, pH 7.4 without or with DEAE- and CM-dextran, respectively. Coacervate droplets: enzyme and substrates are mixed to a suspension of DEAE-/CM-dextran coacervate microdroplets. Bulk coacervate: enzyme and substrates are mixed to the bulk coacervate phase collected after centrifugation of DEAE-/CM-dextran coacervate

microdroplets. **f**, Example of plots showing the increase of the fluorescence intensity over time associated to the conversion of oPD into DAP by C45 (0.25 µM) in the presence of H_2O_2 (1 mM) in pure buffer. The oPD concentration from the lowest to the highest curves is: 0, 10, 20, 35, 50, 75, 100, 200, 500, 700, 1000 µM. RFU: relative fluorescence units. **g**,**h**, Plots of the initial reaction velocity V_0 at increasing oPD concentrations in the different conditions (as labelled); solid dots and error bars represent the average values and standard deviations of three independent measurements, respectively; solid lines show Michaelis-Menten fits. Please note the y-axis scale in **h** is zoomed in compared to **g** to help visualization of the data.

The catalytic efficiency of C45 is enhanced in the coacervate phase

We then investigated the peroxidase activity of C45 in coacervates compared to buffer conditions using the model substrate ortho-phenylenediamine (oPD). In the presence of hydrogen peroxide, oPD is oxidised by C45 into the fluorescent product 2,3-diaminophenazine (DAP). The reaction kinetics can thus be readily monitored by measuring the increase of fluorescence intensity over time.

We first studied the enzyme activity in pure buffer as a reference experiment (**Figures 2a,f**). The enzyme concentration was fixed to 0.25 µM, a condition that met the proportionality between substrate conversion and enzyme concentration (**Supplementary Figure 5**). In addition, since C45 exhibits a relatively high K_M for hydrogen peroxide[22] (K_M = 94 mM), we chose to work at limiting peroxide concentration (1 mM) to minimise peroxide-induced degradation of substrate and enzyme inactivation at low substrate concentrations. While these concentrations were consistent with kinetic analyses performed with other substrates, we selected a buffer pH lower than the optimal value for C45 to ensure coacervate integrity.[22] [24] The plot of the initial reaction velocity obtained at varying oPD concentrations after conversion of the fluorescence signal into DAP concentration using calibration curves (**Supplementary Figure 6**) could be fitted to a simple Michaelis-Menten steady-state model (**Figure 2g**), as reported previously,[22] [24] with a Michaelis-Menten constant, K_M, of 105 ± 7 µM, a maximum rate constant at limiting H_2O_2 conditions, $k' = V_{0,max}/[C45]$, of 8.1 ± 1.2 × 10^{-2} s^{-1}, and a catalytic efficiency, k'/K_M, of 7.7 ± 0.7 × 10^2 $M^{-1}.s^{-1}$ (**Figures 3a-c** and **Table 1**).

This Michaelis-Menten-like peroxidase activity was then used as a platform to test the influence of the coacervates on the enzyme kinetics. We investigated the reaction kinetics in two distinct samples. In the first one, the enzyme and substrates were added to a suspension of coacervate droplets prepared at 3 $mg.mL^{-1}$ of DEAE-dextran and 9 $mg.mL^{-1}$ of CM-dextran (**Figure 2b**). The local concentration of enzyme, H_2O_2, oPD and DAP in the coacervate droplets was therefore dictated by their respective partition coefficients, with species dynamically exchanging between the droplets and the surrounding aqueous phase. We estimated the partition coefficients of oPD and DAP by UV/vis and fluorescence spectroscopy to be 2.9 ± 0.9 and 3.8 ± 1.5, respectively (see Methods), indicating that oPD and DAP were slightly accumulated in the coacervate droplets compared to the surrounding aqueous phase. While we could not determine the partitioning of H_2O_2, it is likely that due to its smaller size and neutral charge it was unselectively distributed in the coacervates and surrounding phase, as already observed for other small neutral molecules such as urea.[28] In the second sample, a bulk coacervate phase was first prepared by centrifugation of a droplets suspension, collected by pipetting, then the enzyme and substrates were added to this dense phase (**Figure 2c**). No up-concentration effect occurred in this case due to the absence of surrounding aqueous phase for proteins and substrates to equilibrate with. By using this bulk coacervate phase, we thus prevented any impact caused by the exchange of substrate, enzyme or product between the surrounding phase and coacervate environment.

In both samples, the total (final) C45 and H_2O_2 concentrations were fixed to their reference values of 0.25 µM and 1 mM, respectively, while the oPD concentration was varied within the chosen range (0 – 1 mM). Importantly, we observed that the bulk coacervate phase affected the DAP fluorescence, therefore calibration curves of DAP fluorescence in the different milieus were systematically used to quantitatively convert fluorescence signals during enzyme reaction into DAP concentration (see Methods and **Supplementary Figure 6**). Plots of the initial velocity vs. oPD concentration after signal conversion to µM of DAP produced per unit time could be well fitted by a Michaelis-Menten steady-state model (**Figure 2g**). The associated Michaelis-Menten constant and kinetic parameters are summarized in **Table 1** and **Figures 3a-c**. Results showed that the presence of coacervate droplets and coacervate bulk phase increased by ca. 2-fold the K_M value while increasing k' by ca. 2-fold and 5-fold, respectively. As a result, the apparent catalytic efficiency, k'/K_M, in the presence of coacervate droplets was comparable to that of C45 in pure buffer, while it was ca. 3-fold higher in the bulk coacervate phase. Note that the larger error bars for the bulk coacervate phase are likely due to the crowdedness and increased viscosity of

this environment that may alter the homogenization of the fluorescence from DAP (especially at the start of the reaction where v_0 is determined).

Observations of the three samples by confocal fluorescence microscopy during the reaction confirmed that the fluorescence signal in the bulk coacervate phase was ca. 6-fold higher than that in buffer after 30 minutes of reaction (**Supplementary Figure 7**). An even higher fluorescence signal was observed within the droplets in the coacervates suspension, due to the partitioning of DAP.

Taken together, our results indicate that the coacervate phase increases the Michaels-Menten constant while increasing the maximum rate constant at limiting H_2O_2 conditions, *k*'. It is worth emphasizing that the bulk coacervate phase results in a higher increase in *k*' compared to the coacervate droplets suspension. This observation suggests that the up-concentration of C45 and oPD within coacervate droplets alone does not account for the increase in *k*', since such an up-concentration effect does not occur in the bulk coacervate phase (see **Figures 3b,c**).

Table 1. Michaelis-Menten parameters of the C45-catalyzed oxidation of oPD with H_2O_2 in different environments.

Condition	K_M (µM)	k' ($\times 10^{-2}$ s^{-1})	k'/K_M ($\times 10^{2}$ $M^{-1}.s^{-1}$)
Buffer	105 ± 7	8.1 ± 1.2	7.7 ± 0.7
Coacervates suspension	185 ± 77	15.5 ± 3.6	9.5 ± 2.8
Bulk coacervate phase	175 ± 27	38.1 ± 15.3	21.0 ± 5.3
CM-dextran, high *c*	90 ± 3	10.0 ± 0.7	11.1 ± 0.7
DEAE-dextran, high *c*	214 ± 19	13.1 ± 0.4	6.1 ± 0.3
DEAE-dextran, low *c*	132 ± 22	6.7 ± 1.4	5.2 ± 1.4

Electrostatic interactions and macromolecular crowding impact the enzyme kinetics

To dissect the underpinning mechanism of the observed increased K_M and increased *k*' in the coacervate environment, we first tested the impact of the coacervate-forming polymers taken separately on the enzyme kinetics. For this purpose, the reaction was performed in the presence of either CM-dextran or DEAE-dextran (**Figures 2d,e**) at a fixed concentration of 75 $mg.mL^{-1}$ (a value close to the polymer concentration in the coacervate phase) and at varying oPD concentrations. Plots of the initial velocity of the enzyme reaction at increasing oPD concentrations after fluorescence signal conversion into DAP concentration using calibration curves were here again fitted with the Michaelis-Menten steady-state model (**Figure 2h**). The resulting kinetics parameters are given in **Table 1** and **Figures 3a-c**. We observed that the presence of DEAE-dextran induced in a 2-fold increase in K_M compared to buffer conditions, namely, a similar effect as the bulk coacervate phase or coacervate droplet suspension. In contrast, the presence of CM-dextran did not alter the K_M value compared to buffer conditions. Similarly, a lower DEAE-dextran concentration (0.1 $mg.mL^{-1}$) did not result in a detectable change in the K_M value compared to buffer conditions (**Supplementary Figure 8** and **Table 1**). These results lead us to assign the increased K_M in the coacervate phase to attractive electrostatic interactions between the enzyme and polycation chains (which local concentration in the coacervate phase is of several tens of $mg.mL^{-1}$), presumably due to a lower accessibility of the enzyme active site upon interacting with the polycation chains.

In addition, both DEAE- and CM-dextran polymers (used at 75 $mg.mL^{-1}$) produced a ca. 1.5-fold increase in the catalytic constant compared to buffer conditions (**Figures 3a-c** and **Table 1**). Since this increase was almost independent on the chemical nature of the polymer used, it was likely due to macromolecular crowding rather than protein/polymer interactions. It is yet worth noting that the *k*' value found in the bulk coacervate phase was almost 4-fold higher than values determined in the presence of either polymer, suggesting that additional contributions from the coacervate local environment beyond crowding, such as electrostatic interactions, played a key role in the enhanced catalytic constant of C45.

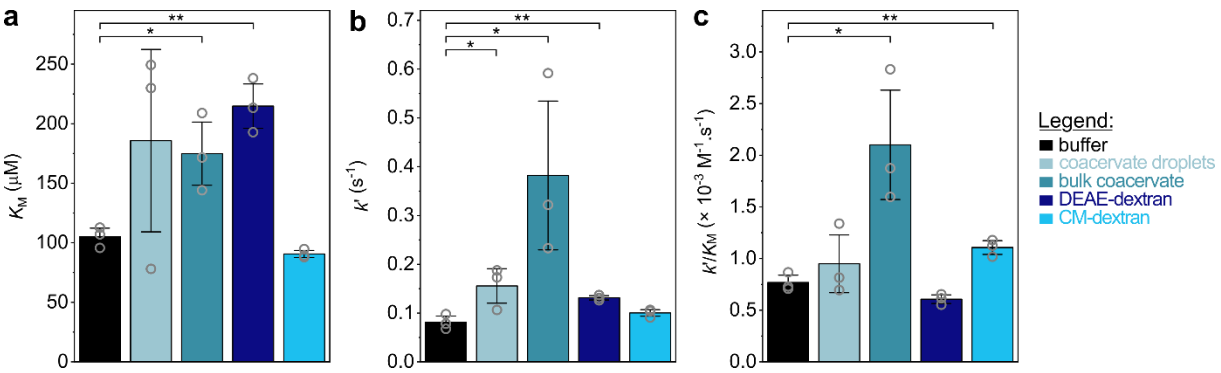

Figure 3. a-c, Plots of the Michaelis-Menten parameters obtained from fits shown in Figures 2g,h: Michaelis-Menten constant K_M (**a**), maximum rate constant at limiting H_2O_2 conditions, $k' = V_{0,max}/[C45]$ (**b**) and catalytic efficiency, k'/K_M (**c**). Boxes and error bars represent the average value and standard deviations of three independent measurements (shown as empty grey circles), respectively. Stars indicate significance: * = p-value < 0.05; ** = p-value < 0.01.

The coacervate phase affects the conformational dynamics of C45

Given the above observations, we last sought to determine possible changes in the structure or dynamics of C45 in the dense coacervate phase using tryptophan fluorescence emission. More specifically, we used the recently reported red-edge excitation shift (REES) phenomenon to explore possible changes in C45 tertiary structure and flexibility in the coacervate environment compared to buffer conditions.[25] The REES effect results in the inhomogeneous broadening of tryptophan emission spectra at decreasing excitation energies, associated with discrete solute-solvent interaction energies increasingly photoselected by the decrease in excitation energy.[29] This effect allows to monitor changes in protein conformational dynamics using tryptophan fluorescence emission.[30-32] Experimentally, the REES effect can be quantified by tracking changes in the centre of spectral mass, CSM, of tryptophan fluorescence emission at increasing excitation wavelength (**Figure 4a-c**). These changes can be modelled using the following equation:

$$CSM = CSM_0 + Ae^{R\Delta\lambda_{ex}} \quad \text{(Equation 1)}$$

where A and R are constants, $\Delta\lambda_{ex}$ is the change in excitation wavelength from 292 nm and CSM_0 is the centre of mass independent of the excitation wavelength. Changes in CSM_0 are typically used to track modifications in tryptophan solvent exposure, hence the tertiary structure of the protein, as an increase in CSM_0 would imply unfolding of the protein.[33] In comparison, for a constant CSM_0 value, previous studies have shown that higher A/R values would signify a broader population of conformational states, hence a higher conformational dynamics and lower protein rigidity.[25] [31, 32]

Interestingly, we observed that the CSM_0 obtained for C45 in buffer and in the coacervate bulk phase were identical (**Figure 4d**), revealing no measurable change in the tertiary structure of the enzyme in the coacervate matrix. This result agrees well with the high conformational stability reported previously for C45 under diverse conditions (temperature,[22] addition or organic solvent[25]). However, a 5-fold decrease of the A/R value was found in the coacervate phase compared to buffer conditions (**Figure 4e**)., pointing to an increased enzyme rigidity in the bulk coacervate environment. This result mirrors the recently reported rigidification of C45 in the presence of an organic co-solvent, 2,2,2-trifluoroethanol (TFE), that also led to a ~~A~~ notable decrease of A/R for a constant CSM_0.[25] Similar to our observations, the study revealed a 6-fold increase in catalytic rate constant under limiting peroxide conditions in the presence of 80% TFE. TFE was further shown to increase the thermal stability of C45 and potentially making it adopt a more active, "natural"-like state.[25] Although we did not investigate in detail the thermodynamics of C45 in the coacervate phase, the REES effect observed in the bulk coacervate phase points to the stabilization of a more rigid conformation of C45, aligning with the mild stabilization of the folded structure of proteins reported in crowded environments,[16c-e] including coacervates.[28]

Overall, our data point to a decrease in C45 conformational dynamics within the coacervate matrix compared to buffer conditions but no alterations in the enzyme tertiary structure. These subtle dynamical changes could contribute to the enhanced enzyme kinetics observed in the coacervate bulk phase.

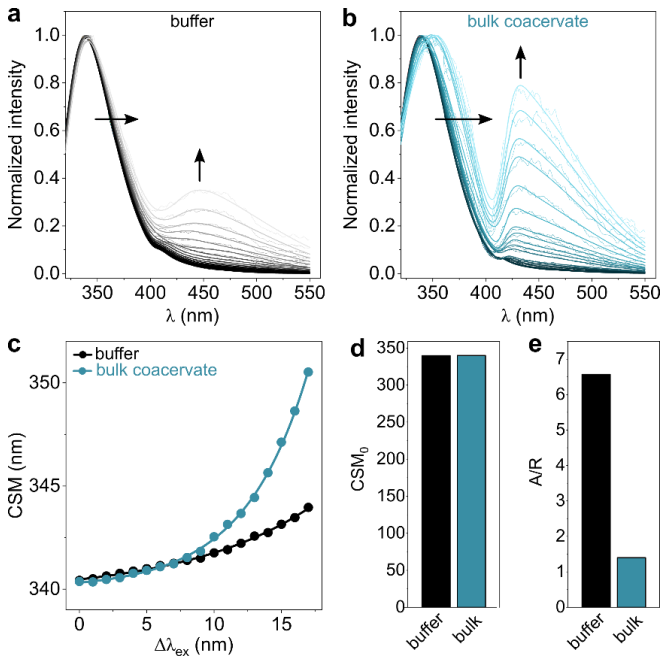

Figure 4. a,**b**, Fluorescence emission spectra of C45 in buffer (**a**) or in the bulk coacervate phase (**b**) at increasing excitation wavelength (292 nm to 309 nm by steps of 1 nm from the darkest to the lightest curve). A red-shift of tryptophan fluorescence emission peak (centred on 340 nm) is observed. **c**, Plot of the centre of spectral mass of tryptophan fluorescence emission as a function of the change in excitation wavelength from 292 nm. Lines represent mono-exponential fits. **d**, Plot of the excitation wavelength-independent centre of mass, CSM_0 (**d**), and of the A/R value (**e**) obtained from the fits in **c**.

Conclusion

To conclude, our results demonstrate that the bulk coacervate phase produced by two oppositely charged polysaccharides leads to a ca. 5-fold enhancement of the catalytic constant of C45, a rationally designed peroxidase. In comparison, only a 2-fold increase in *k'* is observed in a suspension of coacervate droplets, despite the local up-concentration of C45 and its substrate within the droplets via partitioning. At least two reasons can be invoked to account for this discrepancy: one the one hand, the activity of C45 plateaus above a certain concentration (**Supplementary Figure 5**), therefore accumulation of the enzyme in the coacervate droplets may push the reaction into the saturating regime; on the other hand, the product of the reaction also accumulates in the droplets, which can result in product inhibition. In contrast, the bulk coacervate phase is more effective in enhancing the enzyme activity compared to droplets in equilibrium with their surrounding aqueous phase. This phenomenon is attributed to a combination of macromolecular crowding and changes in the enzyme conformational dynamics in the coacervate matrix, without alterations of the native conformation, as reported recently in the presence of an organic co-solvent.[25] This observation further aligns with previously reported effects of molecular crowding on enzyme conformation dynamics.[16a,e] Of course, other contributions, such as local differences in pH, local concentrations of charges and counter-ions, electrostatic interactions,[35] or the lower polarity that has been reported in the interior of coacervates compared to bulk water,[12] [34] cannot be fully discounted.

Overall, quantification of enzyme reactions in bulk coacervate phases appears critical to decouple the different possible contributions of coacervates on enzyme activities, and in particular to disentangle the effect of enzyme and substrate up-concentration from the role of the coacervate matrix itself (crowding, interactions…). Importantly, the law of the mass action may not necessarily lead to a significant increase in catalytic efficiency despite the co-localization and co-accumulation of enzyme and substrate.

Finally, our study exemplifies the relevance of polyelectrolyte-based coacervate systems as simple models to decipher general principles of enzyme catalysis in biomolecular condensates. Our work also provides the first investigation of the activity of a de novo enzyme within coacervates. The simplicity of these helical bundles makes them relatively easy to tailor for specific purposes, e.g., by introducing surface charges to modulate enzyme/polyelectrolyte interactions. Electrostatic interactions have indeed recently been identified to be critical

to modulate enzyme catalysis in coacervates, since weaker polyelectrolyte/protein interactions have been shown to favour higher protein mobility and also higher enzyme activity.[19] Beyond peroxidase-like reactions, C45 catalyses a broad range of transformations such as dehalogenations and carbene-transfer reactions. Coacervates could provide an appealing approach to up-regulate the catalytic efficiency of these reactions for biocatalysis applications both in vivo and in vitro.

Supporting Information

The authors have cited additional references within the Supporting Information.[36 – 39]

Acknowledgements

N.M. acknowledges funding from IdEx Bordeaux (ANR-10-IDEX-03-02), the "Région Nouvelle-Aquitaine" (AAPR 2020-2019-8330510), the "Agence Nationale de la Recherche" (ANR-21-CE06-0022) and the University of Bordeaux RRI "Frontiers of Life". J.L.R.A. acknowledges funding at the University of Bristol from the Leverhulme Trust (RPG-2020-002) and the Biological and Biotechnological Sciences Research council (BB/R016445/1).

Keywords: coacervates • de novo enzymes • membraneless organelles • biocatalysis

References

[1] S. F. Banani, H. O. Lee, A. A. Hyman, M. K. Rosen, *Nat. Rev. Mol. Cell Biol.* **2022**, *18*, 285-298.
[2] B.G. O'Flynn, T. Mittag, *Curr. Opin. Cell Biol.* **2021**, *69*, 70-79.
[3] Y. Zhang, G. J. Narlikar, T.G. Kutateladze, *J. Mol. Biol.* **2021**, *433*, 166624.
[4] Y. Dai, L. You, A. Chilkoti, *Nat. Rev. Bioeng.* **2023**, *1*, 466-480.
[5] S. Lim, D. S. Clark, *Trends Biotechnol.* Accepted, DOI: 10.1016/j.tibtech.2023.10.003
[6] E. M. Zhao, N. Suek, M. Z. Wilson, E. Dine, N. L. Pannucci, Z. Gitai, J. L. Avalos, J. E. Toettcher, *Nat. Chem. Biol.*, **2019**, *15*, 589-597.
[7] N. A. Yewdall, A. A. M. André, T. Liu, E. Spruijt, *Curr. Opin. Colloid Int. Sci.*, **2021**, *52*, 101416.
[8] Z. Lin, T. Beneyton, J.-C. Baret, N. Martin, *Small Methods*, **2023**, *7*, 2300496
[9] H. Karoui, M. J. Seck, N. Martin, *Chem. Sci.*, **2021**, *12*, 2794-2802 (2021)
[10] K. A. Black, D. Priftis, S. L. Perry, J. Yip, W. Y. Byun, M. Tirrell, *ACS Macro Lett.*, **2014**, *3*, 1088-1091.
[11] a) W. C. Blocher McTigue, S. L. Perry, *Small*, **2020**, *16*, 1907671; b) Biplab. K.C., T. Nii, T. Mori, Y. Katayama, A. Kishimura, *Chem. Sci.*, **2023**, *14*, 6608-6620.
[12] S. Koga, D. Williams, A. Perriman, S. Mann, *Nat. Chem.*, **2011**, *3*, 720-724.
[13] C. Strulson, R. Molden, C. Keating, P. Bevilacqua, *Nat. Chem.*, **2012**, *4*, 941-946.
[14] a) C. Love, J. Steinkühler, D. T. Gonzales, N. Yandrapalli, T. Robinson, R. Dimova, T.-Y. D. Tang, *Angew. Chem. Int. Ed.*, **2020**, *59*, 5950-5957; b) Y. Chen, M. Yuan, Y. Zhang, S. Liu, X. Yang, K. Wang, J. Liu, *Chem. Sci.*, **2020**, *11*, 8617-8625.
[15] N. A. Yewdall, B. C. Buddingh, W.J. Altenburg, S. B. P. E. Timmermans, D. F. M. Vervoort, L. K. E. A. Abdelmohsen, A. F. Mason, J. C. M. van Hest, *ChemBioChem*, **2019**, *15*, 2643-2652.
[16] a) C. Alfano, Y. Fichou, K. Huber, M. Weiss, E. Spruijt, S. Ebbinghaus, G. De Luca, M. Agnese Morando, V. Vetri, P. A. Temussi, A. Pastore, *Chem. Rev.*, **2024**, *124*, 3186-3219. b) E. Solokova, E. Spruijt, M.M.H. Hansen, W.T.S. Huck, *Proc. Natl. Acad. Sci.*, **2013**, *110*, 11692-11697; c) A. C. Miklos, M. Sarkar, Y. Wang, G.J. Pielak, *J. Am. Chem. Soc.* **2011**, *133*, 18, 7116-7120; d) N. Tokuriki, M. Kinjo, S. Negi, M. Hoshino, Y. Goto, I. Urabe, T. Yomo, *Protein Sci.*, **2004**, *13*, 125-133; e) I. T. Chu; B. O. Hutcheson, H. R. Malsch, G. J. Pielak, *J. Phys. Chem. Lett.* **2023**, *14,* 2599-2605
[17] T. Kojima, S. Takayama, *ACS Appl. Mater. Interfaces*, **2018**, *10*, 32792-32791.
[18] B. Drobot, J. M. Iglesias-Artola, K. Le Vay, V. Mayr, M. Kar, M. Kreysing, H. Mutschler, T.-Y.D. Tang, *Nat. Commun.*, **2018**, *9*, 3643.

[19] A. B. Cook, B. Delgado Gonzalez, J. C. M. van Hest, *Biomacromolecules*, **2024**, *25*, 425-435.
[20] W. Peeples, M. K. Rosen, *Nat. Chem. Biol.*, **2021**, *17*, 693-702.
[21] T. Beneyton, C. Love, M. Girault, T.-Y.D. Tang, J.-C. Baret, *ChemSystemsChem*, **2020**, *2*, e2000022.
[22] D. W. Watkins, J. M. X. Jenkins, K. J. Grayson, N. Wood, J. W. Steventon, K. K. Le Vay, M. I. Goodwin, A. S. Mullen, H. J. Bailey, M. P. Crump, F. MacMillan, A. J. Mulholland, G. Cameron, R. B. Sessions, S. Mann, J. L. R. Anderson, *Nat. Commun.* **2017**, *8*, 358.
[23] R. Stenner, J. W. Steventon, A. Seddon, J. L. R. Anderson, *Proc. Natl. Acad. Sci.*, **2020**, *117*, 1419-1428.
[24] J. M. X. Jenkins, C. E. N. Noble, K. J. Grayson, A. J. Mulholland, J. L. R. Anderson, *J. Inorg. Biochem.*, **2021**, *217*, 111370.
[25] S. A. Hindson, H. A. Bunzel, B. Frank, D. A. Svistunenko, C. Williams, M. W. van der Kamp, A. J. Mulholland, C. R. Pudney, J. L. R. Anderson, *ACS Catal.*, **2021**, *11*, 11532-11541.
[26] H. Wang, F. M. Kelley, D. Milanovic, B. S. Schuster, Z. Shi, *Biophys. Rep.*, **2021**, *1*, 100011.
[27] R. A. Kapelner, V. Yeong, A. C. Obermeyer, *Curr. Opin. Colloid Int. Sci.*, **2021**, *52*, 101407.
[28] N. Martin, M. Li, S. Mann, *Langmuir*, **2016**, *32*, 5881-5889.
[29] A. Chattopadhyay, S. Haldar, *Acc. Chem. Res.*, **2014**, *47*, 12-19.
[30] D. A. M. Catici, H. E. Amos, Y. Yang, J. M. H. van den Elsen, C. R. Pudney, *FEBS J.*, **2016**, *283* , 2272-2284
[31] H. B. L. Jones, S. A. Wells, E. J. Prentice, A. Kwok, L. L. Liang, V. L. Arcus, C. R. Pudney, *FEBS J.*, **2017**, *284*, 2829-2842.
[32] M. J. Knight, R. E. Wolley, A. Kwok, S. Parsons, H. B. L. Jones, C. E. Gulácsy, P. Phaal, O. Kassaar, K. Dawkins, E. Rodriguez, A. Marques, L. Bowsher, S. A. Wells, A. Watts, J. M. H. van den Elsen, A. Turner, J. O'Hara, C. R. Pudney, *Biochem. J.*, **2020**, *477*, 3599-3612.
[33] Y.K. Reshetnyak, Y. Koshevnik, E.A. Burstein, *Biophys. J.*, **2001**, *81*, 1735-1758.
[34] U. Capasso Palmiero, C. Paganini, M. R. G. Kopp, M. Linsenmeier, A. M. Küffner, P. Arosio, *Adv. Mater.*, **2022**, *34*, 2104837.
[35] J. Xia, P.L. Dubin, Protein-Polyelectrolyte Complexes in Macromolecular Complexes in Chemistry and Biology, **1994**, Springer Berlin, Heidelberg
[36] C. P. Brangwynne, T. J. Mitchison, A. A. Hyman, *Proc. Natl. Acad. Sci.*, **2011**, *108*, 4334-4339.
[37] R. D. Phair, S. A. Gorski, T. Misteli, *Methods Enzymol*. **2003**, *375*, 393-414.
[38] W. M. Aumiller Jr, F. Pir Cakmak, B. W. Davis, C. D. Keating, *Langmuir*, **2016**, *32*, 10042-10053.
[39] D. Axelrod, D. E. Koppel, J. Schlessinger, E. Elson, W. W. Webb, *Biophys. J.* **1976**, *16*, 1055-1